JOURNAL OF AIRCRAFT
Vol. 40, No. 5, September–October 2003

Engineering Notes

ENGINEERING NOTES are short manuscripts describing new developments or important results of a preliminary nature. These Notes cannot exceed 6 manuscript pages and 3 figures; a page of text may be substituted for a figure and vice versa. After informal review by the editors, they may be published within a few months of the date of receipt. Style requirements are the same as for regular contributions (see inside back cover).

Active Transparent Stall Control System for Air Vehicles

Mehul P. Patel*
Orbital Research, Inc., Cleveland, Ohio 44143
Carl P. Tilmann†
U.S. Air Force Research Laboratory, Wright–Patterson Air Force Base, Ohio 45433
and
T. Terry Ng‡
University of Toledo, Toledo, Ohio 43606

Introduction

THE primary cause of aircraft stall is the separation of airflow over the surface of the wings, which occurs at relatively high angles of attack α due to a combination of viscous forces and adverse pressure gradients acting within the boundary layer. Also, unsteady flow environment and high external flow turbulence encountered over the wings' surface during a dynamic maneuver, forces early flow separation, causing the aircraft to stall at an angle of attack much lower than the calibrated stall angle. To broaden the operational flight envelope, and to improve maneuverability of aircraft, it is desired to enhance the performance of the wings and other aerodynamic control surfaces.

Recent advances in microelectromechanical systems technology for fluid mechanical systems has enabled active flow-control strategies for scores of aerodynamic and hydrodynamic applications.[1,2] One of the flow-control techniques that is currently employed on today's aircraft utilizes passive vortex generators (VGs) for enhancing the aerodynamic performance of the wings by controlling flow separation, a concept pioneered by Lin et al.[3] VGs energize the boundary layer via enhanced momentum mixing that forces flow reattachment and delays separation. Passive VGs are highly effective in controlling separation; however, steady deployment of VGs at cruise conditions, where no control is required, produce sizeable parasitic drag.[4]

Many researchers have investigated the potential of VGs for separation control; nonetheless, most of the work has focused primarily on passive VGs. This Note presents proof-of-concept development of an autonomous active stall control system for air vehicles, using deployable flow effectors (DFEs), that is, active VGs, coupled with a system of embedded pressure sensors and a feedback controller.

Received 7 December 2002; revision received 2 May 2003; accepted for publication 2 May 2003.

*Senior Aerodynamicist, Aerodynamics Group. Member AIAA.
†Senior Research Engineer, Air Vehicles Directorate. Senior Member AIAA.
‡Professor, Department of Mechanical, Industrial, and Manufacturing Engineering. Senior Member AIAA.

This research leads to the realization of a smart-wing concept,[5] where 1) the control system deploys DFEs only when required, lowering parasitic drag; 2) the system is transparent to the actual flight-control system, minimizing system complexity and overall cost of implementing smart-wing modules; and 3) the system detects actual physical stall of the wing rather than relying on the calibrated stall angles.

DFEs

DFEs are active VGs that promote near-wall flow mixing to energize the boundary layer, which in turn delays flow separation, leading to pressure recovery and an overall increase in the wing lift. DFE configurations used in this study were based on the findings of previous research, which was focused on optimizing DFE parameters to increase maximum lift coefficient $C_{L,\max}$ of the wing via controlling flow separation.[6,7] DFEs utilized in the present study were made from epoxy glass–fabric board in the form of small mechanical tabs of length $l = 9$ mm, width $w = 0.8$ mm, and height $h = 3$ mm. They were flush mounted on the surface of the wing, nonobtrusive to the flow, and were deployed approximately 1 mm outside the boundary layer when triggered by the controller. Two DFE-strips, each consisting five pairs of skewed DFEs that produce counter-rotating vortices, were flush mounted at 2.7% chord c of the wing.

Transparent Stall Control Technique

An active transparent stall control system utilizing sensors, actuators, and a closed-loop controller was designed and tested on a NACA 0020 wing model in a low-speed wind tunnel. The main objective of the control system was to enable active detection and control of local flow separation, using a system of fast-response (500-Hz) pressure sensors, DFEs, and a feedback controller, to delay wing stall. The method of predicting flow separation was based

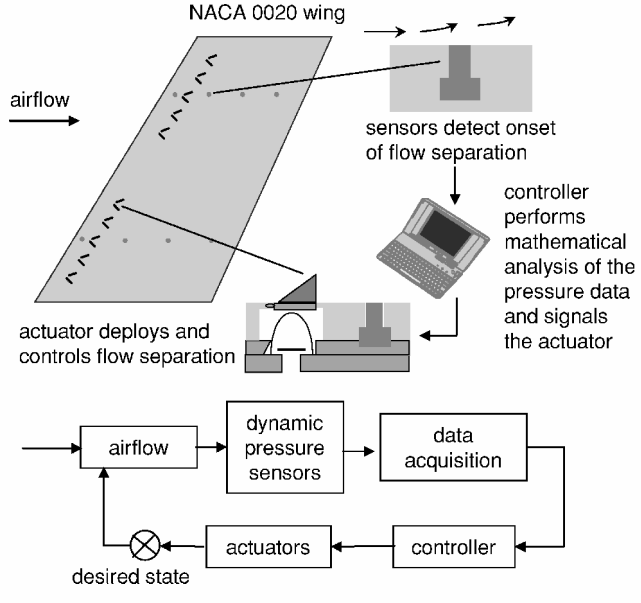

Fig. 1 Underlying principle of smart-wing concept.

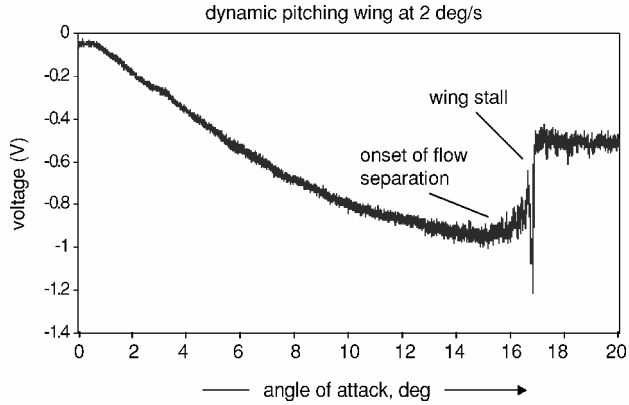

Fig. 2 Typical response from a dynamic pressure sensor located near leading edge of a pitching wing.

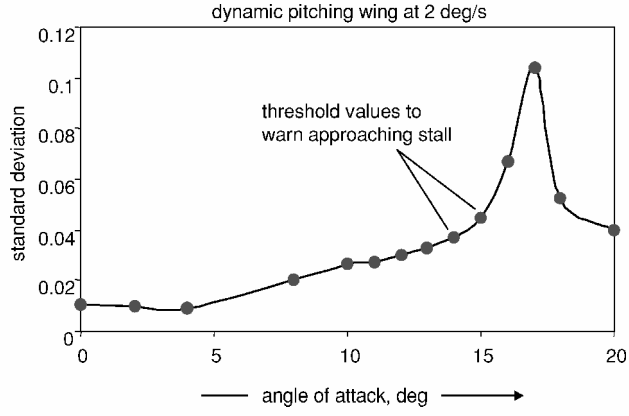

Fig. 3 Characteristic behavior of STDEV pressure fluctuations captured from dynamic pressure sensor located near the leading edge of a pitching wing.

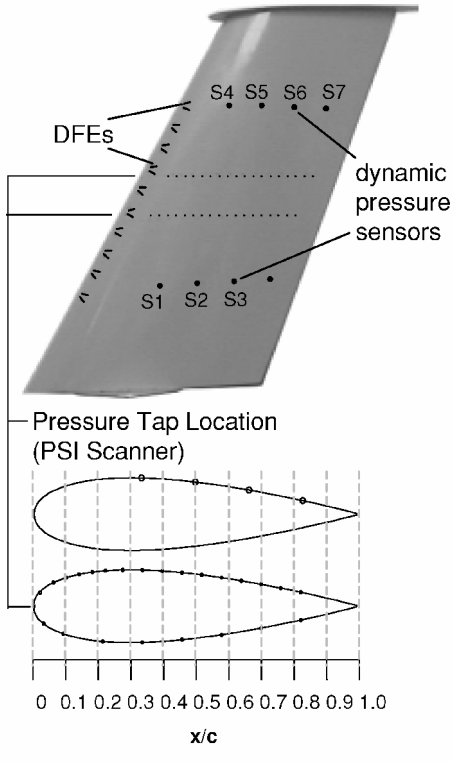

Fig. 4 NACA 0020 wing model with 71.12-cm wing span, 48.26-cm root, and 35.96-cm tip.

on the identification of characteristic shifts in the power spectrum of the pressure fluctuations in the vicinity of flow separation. The underlying principle of a smart-wing concept that utilizes the transparent stall control technique is shown in Fig. 1. Abrupt shifts in the pressure data, captured as spikes in standard deviation (STDEV) of surface pressures, created a characteristic signature of imminent flow separation, which served as the trigger for activation of DFEs. Pressure fluctuations captured from a fast-response (sampling rate

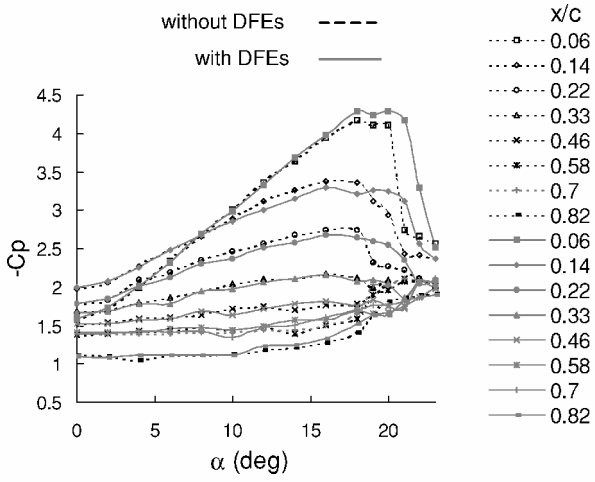

Fig. 5 Pressure coefficient $-C_p$ vs α on NACA 0020 wing: – – –, without DFEs; ——, with DFEs; □ and ■, $x/c = 0.06$; ◇ and ♦, $x/c = 0.14$; ○ and ●, $x/c = 0.22$; △ and ▲, $x/c = 0.33$; x, $x/c = 0.46$; ∗, $x/c = 0.58$; +, $x/c = 0.7$ and ■, $x/c = 0.82$.

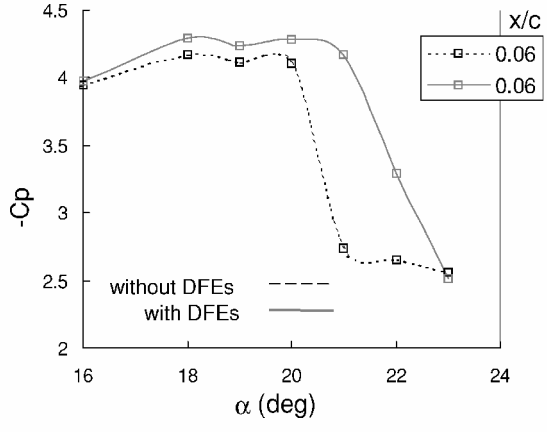

Fig. 6 Pressure coefficient $-C_p$ vs α at $x/c = 0.06$ on NACA 0020 wing with DFEs and without DFEs.

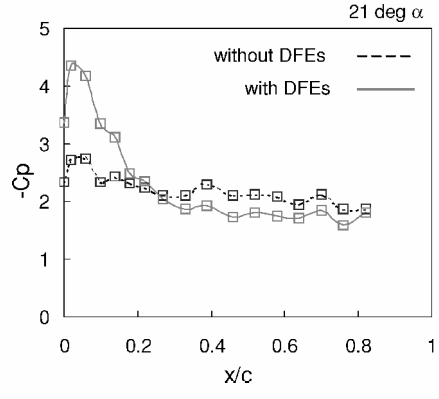

Fig. 7 Pressure coefficient $-C_p$ vs x/c at 21 deg α on NACA 0020 wing with DFEs and without DFEs.

500-Hz) pressure sensor located at 10%c of a PE 1423 pitching airfoil (pitch rate of 2 deg/s) are plotted vs time in Fig. 2 and the corresponding STDEV plot is shown in Fig. 3. Based on these observations, the controller architecture for this study was extended to include a memory unit that stored, for a variety of flow conditions, threshold values of the tracking parameter, STDEV, from different pressure sensors located on the wing's surface. The controller detected characteristic shifts of the pressure data by monitoring STDEV values and deployed DFEs in a preassigned configuration, when the current STDEV values crossed the threshold values. In summary, detection of incipient stall was achieved solely through mathematical analysis of pressure fluctuations recorded from pressure sensors that were embedded flush to the surface of the wing. Consequently, only a single fast-response pressure sensor located optimally on the surface of the wing can be used for stall detection.

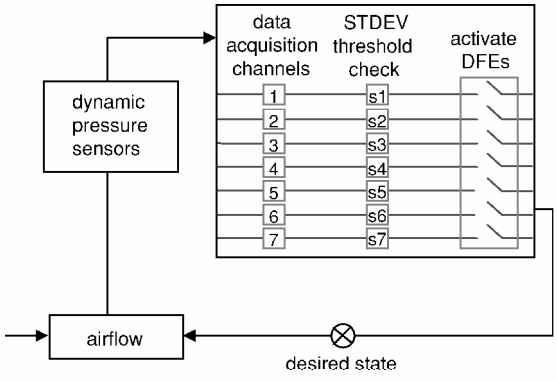

Fig. 8 Control-law flowchart for closed-loop experiments.

Wing Model

A NACA 0020 wing with a chord length c-48.26 cm at the root and 35.96 cm at the tip, resulting in a taper ratio of 1.3, span of 71.12 cm, and a 30-deg sweep, with a constant 20% maximum thickness in the streamwise direction was fabricated (Fig. 4). The model was integrated with 1) 10 pairs of DFEs located spanwise at 2.7%c; 2) two spanwise rows at 33.3% and 66.6% span from the wing root, consisting four fast-response pressure sensors at 33.3, 50, 66.6, and 83.3%c from the leading edge; and 3) static pressure ports on the top and bottom surfaces of the wing.

Wind-Tunnel Tests and Experimental Uncertainty

Tests were performed at the University of Toledo, Fluids Dynamics Laboratory in a 0.9×0.9 m closed-loop, low-speed wind tunnel. The flow in the test section was uniform with a turbulence level of 0.2% outside of wall boundary layers. All experiments were performed at Reynolds number $Re = 0.6 \times 10^6$ for α ranging from 0 to 23 deg with increments of 2 deg. Static tests were conducted on both

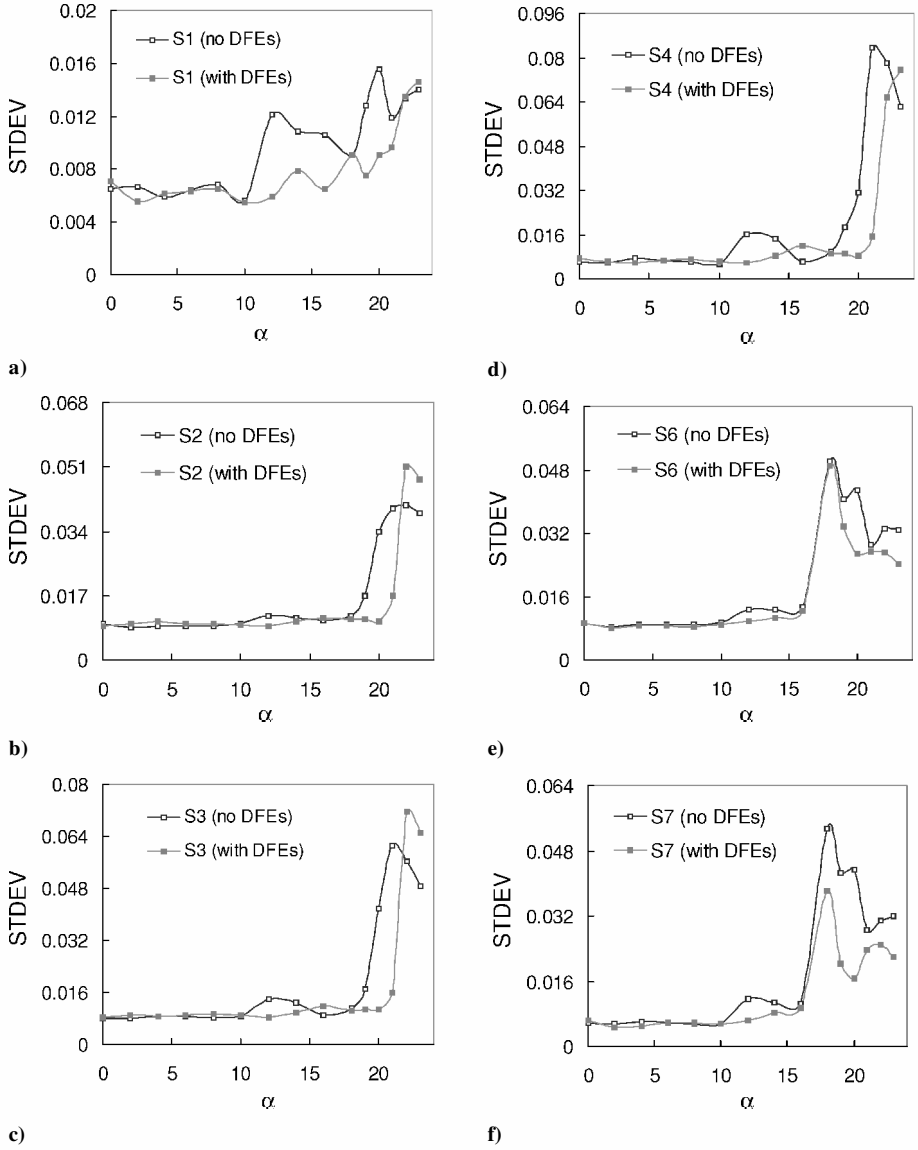

Fig. 9 STDEV pressure fluctuations captured from sensors —S1, S2, S3, S4, S6, and S7 for varying α of the NACA 0020 wing model, with and without DFEs.

clean-wing (no DFEs) and smart-wing (DFEs deployed at 2.7%c) configurations, to demonstrate the effectiveness of DFEs in controlling leading-edge flow separation and also to capture the required unsteady pressure fluctuations using fast-response pressure sensors for the development of closed-loop control system. Dynamic tests were conducted by pitching the wing from $\alpha = 0$ to 23 deg at the rate of 2 deg/s. The purpose of dynamic-pitching tests was to demonstrate the ability of the active stall control system in delaying wing stall during a dynamic environment.

There were two sources of uncertainty in the experiments. One from the turntable used for positioning the wing at a given α and second from the pressure readings. The α-positioning turntable was incorporated with an optical encoder feedback that offered accuracy up to 1 arc-s, axis wobble of less than 2 arc-s, and a repeatability of 0.2 arc-s. Accuracy of pressure data was verified by repeated measurements, for both static and dynamic tests, that showed good repeatability.

Results and Discussion

Results are presented in the form of pressure coefficient C_p variation on the upper surface of the wing for both clean-wing and smart-wing configurations, to demonstrate the effect of DFEs. Results from incipient stall control experiments are presented by plotting STDEV of raw pressure data for both clean and smart configurations. Figure 5 shows the effect of DFEs on the pressure coefficient C_p along the upper surface of the wing for different α states. Because of the characteristic nature of the NACA 0020 tapered wing, the flow was attached over the large portion of upper surface of the wing, that is, for α up to 18 deg. It was observed that, as α was increased from 0 to 23 deg, the effectiveness of DFEs progressively increased. This was because, as α increased, flow separation successively progressed from the trailing edge toward the leading edge of the wing, within the proximity of DFE's zone of influence. For the case with clean wing, where no DFEs were deployed, incipient stall as indicated by the decrease in the C_p slope was observed at $\alpha = 18$ deg, and complete stall of the wing was observed between $\alpha = 19$ and 20 deg. For the smart-wing configuration, that is, DFEs deployed at 2.7%c, the DFEs were highly effective in controlling leading-edge flow separation and, therefore, delaying wing stall for conditions beyond $\alpha = 18$ deg, shown in Fig. 5. The surface pressures near the leading edge at 0.06c, as shown in Fig. 6, indicate that DFEs were most effective near $\alpha = 21$ deg, where they increased local suction by over 50%. Figure 7 shows C_p variation at different chord locations at $\alpha = 21$ deg for both clean- and smart-wing configurations. As shown in Fig. 7, at $\alpha = 21$ deg, DFEs demonstrate a large flow effect between regions from the leading edge to 0.2c of the wing. In summary, results from DFE-characterization tests provided valuable information about the level of effectiveness of DFEs in controlling leading-edge flow separation and its subsequent effect in delaying wing stall at low speeds. During these tests, data from dynamic (fast-response, 500-Hz) pressure sensors were also recorded to obtain STDEV thresholds for the stall control system, to be used for the dynamic-pitching experiments, which are discussed in the following section.

A simple schematic of the control law used in the feedback controller for active stall control system is shown in Fig. 8. Threshold values of the incipient stall tracking parameter, STDEV, for different α and all pressure sensors were determined from static experiments conducted on the clean-wing configuration. Figure 9 shows comparison of STDEV of pressure data from six different fast-response pressure sensors for both clean- and smart-wing configurations from $\alpha = 0$ to 24 deg in increments of 2 deg. The locations of pressure sensors are presented in Table 1. Plots show that, as α increased, STDEV of the pressure data also increased steadily, until prestall conditions, that is, $\alpha = 18$ deg, where a characteristic spike in STDEV values was observed. For all cases, the DFEs were successfully able to control flow separation as indicated by a delay in the SDTEV spike as shown in Fig. 9, which correlates to the high vales of $-C_p$ in Figs. 5 and 6.

Dynamic pitching tests from $\alpha = 0$ to 23 deg at a pitching rate of 2 deg/s were conducted to demonstrate the ability of the active

Table 1 Location of dynamic pressure sensors

Sensors	x/c	Wing span
S1	0.33	33%
S2	0.50	33%
S3	0.66	33%
S4	0.33	66%
S5	0.50	66%
S6	0.66	66%
S7	0.83	0.83

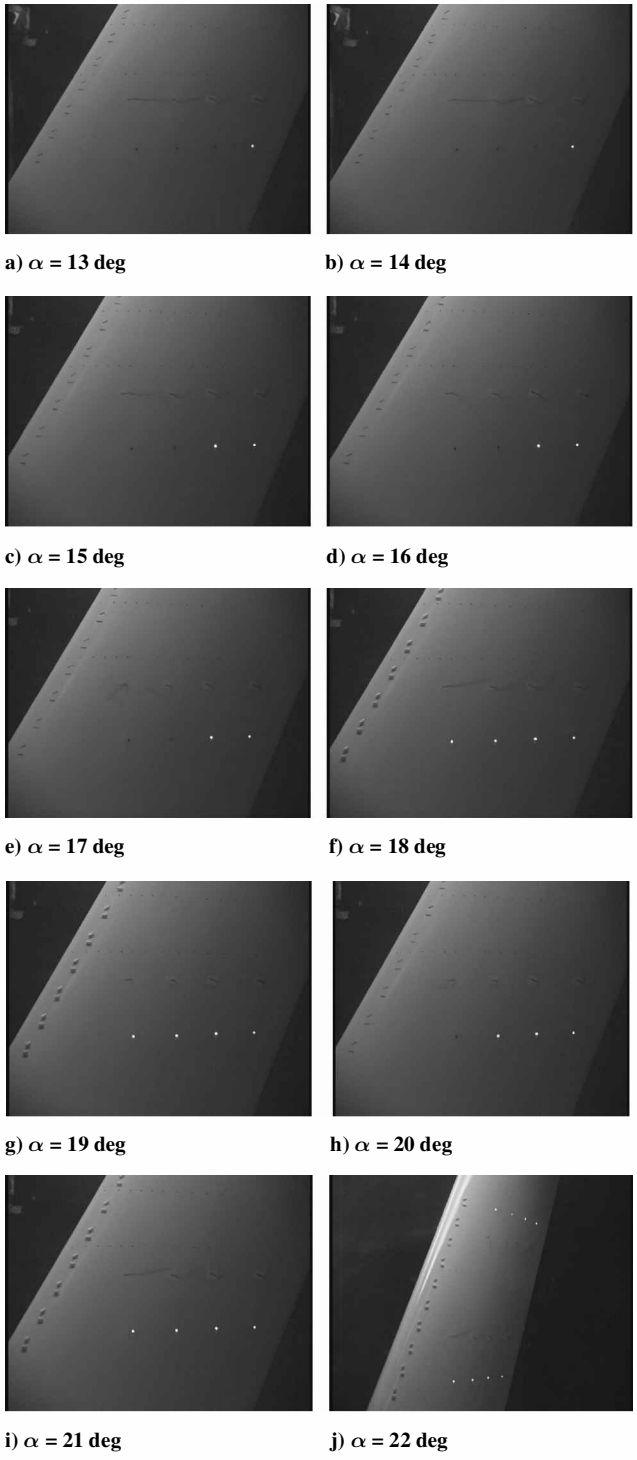

a) α = 13 deg **b) α = 14 deg**

c) α = 15 deg **d) α = 16 deg**

e) α = 17 deg **f) α = 18 deg**

g) α = 19 deg **h) α = 20 deg**

i) α = 21 deg **j) α = 22 deg**

Fig. 10 Snapshots from the closed-loop flow control demonstration on NACA 0020 wing model.

stall control system to delay wing stall in an unsteady environment. Pressure sensors S1 and S5, location shown in Table 1, were used by the controller in the closed-loop flow control demonstration. During the α sweep of the wing at 2 deg/s, it was observed that with increasing α, flow separation successively progressed from the trailing edge toward the leading edge of the wing, as shown in a series of snapshots in Fig. 10. Figure 10 shows that, as α was increased from 13 to 23 deg, the pressure sensors, which are represented by light emitting diodes, lit up at the trailing edge before those at the leading edge, confirming the STDEV-based control law for detection of critical flow conditions. As can be inferred from Fig. 10, leading-edge separation occurred at $\alpha = 18$ deg. The controller triggered the actuation of DFEs at $\alpha = 18$ deg, forcing flow reattachment and a delay in stall angle up to $\alpha = 20$ deg. For $\alpha \geq 21$ deg, the wing was completely stalled, and the DFEs had no effect on the fluid flow.

The results presented in this Note are for a low Reynolds number incompressible flow case where the influence of three-dimensional flow caused due to wing sweep and wing taper on the reliability of STDEV technique are not fully examined. Nevertheless, it is shown that the frequency characteristics of imminent flow separation is a function of sensor location on the wing surface, and these characteristics transpire into flow-separation signature in the form of STDEV thresholds, which are distinct for each sensor location. As this approach evolves further, advanced signal processing techniques such as a recursively fit autoregressive moving average exogenous system identification model or the short-time Fourier transform model will be used to create more sophisticated stall signature definitions for three-dimensional crossflow conditions. As for dynamic maneuvers, modular arrays of colocated sensors, actuators, and local controllers will need to be coordinated to maintain a desired flow effect.

Conclusions

Proof-of-concept experiments for an active transparent stall control system were successfully conducted on a 30-deg sweep NACA 0020 wing in a low-speed wind tunnel. The control system consisted of fast-response pressure sensors, deployable flow control devices, and a closed-loop controller. Findings on the distinctive nature of pressure fluctuations during prestall conditions served as the actuating signal for the controller to trigger the leading-edge flow control devices. Results from open-loop experiments demonstrated significant increase in the upper surface suction levels before wing stall, causing a delay in the stall angle. Closed-loop experiments demonstrated the ability of the controller to detect actively the onset of wing stall and employed flow effectors to control separation and delay stall, in real time. Successful application of such transparent stall control systems on control surfaces will lead to improved aerodynamic performance of both conventional and unconventional air vehicles.

Acknowledgments

The authors thank Frederick Lisy, Troy Prince, Jack DiCocco, and Reed Carver of Orbital Research, Inc., for supporting portions of this research under Grant F33615-99-C-3008 from the U.S. Air Force Research Laboratory at Wright–Patterson Air Force Base.

References

[1]Gad-el-Hak, M., *Flow Control: Passive, Active, and Reactive Flow Management*, 1st ed., Cambridge Univ. Press, Cambridge, England, U.K., 2000, pp. 150–188.

[2]McMichael, J. M., "Progress and Prospects of Active Flow Control Using Microfabricated Electromechanical Systems," AIAA Paper 96-0306, Jan. 1996.

[3]Lin, J. C., Robinson, S. K., McGhee, R. J., and Valarezo, W. O., "Separation Control on High-Lift Airfoils Via Micro-Vortex Generators," *Journal of Aircraft*, Vol. 31, No. 6, 1994, pp. 1317–1323.

[4]Schmidt, R., and Fellenstein, J., "Microactuator Arrays for Adaptable Control Surfaces," Final Rept., Advanced Research Projects Agency, Ord. No. 5916, U.S. Army Missile Command, Contract DAAH01-92-C-R207, 1992.

[5]Lisy, F. J., Carver, R., and Prince, T. S., "Smart Surfaces For Flow Control Arrays," Final Rept., Phase I U.S. Air Force Small Business Innovation Research Contract F33615-98-C-3006, Jan. 1999.

[6]Patel, M. P., Carver, R., Lisy, F. J., Prince, T. S., and Ng, T. T., "Detection and Control of Flow Separation Using Pressure Sensors and Micro-Vortex Generators," AIAA Paper 2002-0268, Jan. 2002.

[7]Patel, M. P., Prince, T. S., Ng, T. T., and Lisy, F. J., "Control of Aircraft Stall via Embedded Pressure Sensors and Deployable Flow Effectors," AIAA Paper 2002-3170, June 2002.

Navier–Stokes-Based Study into Linearity in Transonic Flow for Flutter Analysis

Roberto G. A. Silva,* Olympio A. F. Mello,† and João L. F. Azevedo‡
Centro Técnico Aeroespacial, 12228-904 São José dos Campos SP, Brazil

Introduction

IT has been known for quite some time[1] that transonic flow conditions are critical for flutter, with the flutter dynamic pressure being substantially reduced for Mach numbers near unity, in a phenomenon usually termed as "transonic dip."[2] The severity of flutter at transonic speeds is linked to the presence of moving shock waves over the wing surface.[3] From these considerations it is clear that accurate flutter predictions depend on the ability of predicting correct shock strength and location in a time-accurate fashion. In recent years there has been increased emphasis on the use of computational-fluid-dynamics procedures to accomplish such task.

Most flutter computations use commercial finite element codes with aeroelastic modeling capability such as NASTRAN™. These codes, however, are usually based on linear aerodynamic methods and thus limited to subsonic or supersonic analysis. Transonic flutter clearance relies on experience combined with costly and time-consuming wind tunnel and/or flight tests. More recently, computational aeroelasticity has allowed coupled aerodynamic/structural dynamic computations in the transonic regime. However, the computational resources needed for this coupled analysis are quite significant, and so its industrial application is still limited.[4]

Efforts to provide viable alternatives to these costly analyses and tests have been reported in the literature. These methods approximately model transonic nonlinear aerodynamics and are based on corrections of the linear aerodynamic influence coefficient matrix. The Transonic Equivalent Strip method (TES)[5] is one approach that shows good results in predicting the transonic dip phenomenon. The TES method is based on the application of two consecutive correction steps: chordwise (mean flow) and spanwise (phase correction) to a given steady mean pressure input from measured or computed data. Another approach is the local equivalence concept,[6] which is based in an optimization procedure using computed or wind-tunnel results.

Pitt and Goodman[7] developed modifications of doublet-lattice influence coefficients using results from a transonic-small-disturbance code. That method was capable of simulating the transonic dip phenomenon with small differences with respect to wind-tunnel data.

Received 25 November 2002; revision received 13 May 2003; accepted for publication 14 May 2003.

*Research Engineer, Aeronautical Systems Division, Instituto de Aeronáutica e Espaço; rasilva@iae.cta.br.

†Senior Research Engineer, Instituto de Aeronáutica e Espaço; oamello@iae.cta.br.

‡Senior Research Engineer, Head of Aerodynamics Sub-Division, Space Systems Division, Instituto de Aeronáutica e Espaço. Senior Member AIAA.